SUPPLEMENTAL MATERIAL

Supplemental Methods

Molecular Biology

All mutagenesis was performed using the overlap extension polymerase chain reaction (PCR) with Phusion Hot Start Flex Kit (New England Biolabs) and primers from Sigma-Aldrich. PCR products were ligated into the parent plasmid using T4 DNA ligase (New England Biolabs) and were chemically transformed into Turbo Competent cells (New England Biolabs). Multiple clones were selected and plasmids were isolated using the NucleoSpin Plasmid miniprep kit (Macherey-Nagel). Samples were then sequenced to select a single clone for Midiprep (NucleoBond Xtra Midi, Macherey-Nagel). Each construct was then linearized and purified with the NucleoSpin Gel and PCR Clean-up kit (Macherey-Nagel). Finally, capped mRNA was synthesized (mMessage mMachine T7 Transcription Kit, Life Technologies).

Xenopus Laevis

Oocyte harvest was performed on *Xenopus Laevis* (Nasco) no more than four times (~25 frogs). During the oocyte harvest procedure, distress was minimized by anesthetizing frogs in water containing 0.2% tricaine (3-aminobenzoic acid ethyl ester, methane sulfonate salt). After oocyte harvest, the wound was sutured while the frog is still anesthetized, according to our protocols that were approved by the Institutional Animal Care and Use Committee and in accordance with NIH guidelines.

Cut-open oocyte recording

cRNAs for the human β_1 subunit (UniProtKB/Swiss-Prot accession no. Q07699.1) and α-subunit $Na_V1.5$ (accession no. Q14524.1) were produced from the pBSTA and pMAX vectors (respectively) and injected at a 2:1 molar ratio (50 ng per cell total) into *Xenopus laevis* oocytes. Oocytes were incubated at 18°C for 2–7 d in solution with (mM) 93 NaCl, 5 KCl, 1.8 $CaCl_2$, 1 $MgCl_2$, 5 HEPES, and 2.5 Na-pyruvate, and 1% penicillin-streptomycin, pH 7.4. Cut-open oocyte recordings[1, 2] were performed using an amplifier (CA-1B; Dagan Corporation) coupled to an A/D converter (Digidata 1440; Molecular Devices) with Clampex and Clampfit software (v10; Molecular Devices) for acquisition and analysis. Temperature was maintained at 19°C with a controller (HCC-100A; Dagan Corporation). The internal solution was (mM): 105 NMG-Mes, 10 Na-Mes, 20 HEPES, and 2 EGTA, pH 7.4. The external solution was composed of (mM): 25 NMG-Mes, 90 Na-Mes, 20 HEPES, and 2 $Ca\text{-}Mes_2$, pH 7.4. For gating currents, Na-Mes was replaced by NMG-Mes in both the external and internal solutions and the external solution contained 10 μM TTX.

Data was collected with standard I-V protocols by simultaneous recording of the ionic current and the fluorescence signal from the labeled domain to construct the voltage dependence of steady-state activation (G-V) and voltage dependence of VS movement (F-V) functions. Cells were depolarized in 10 or 20 mV increments from a holding potential of -100 mV. Depolarizing pulses were preceded by a 100-ms-long prepulse and 50-ms-long postpulse to -120 mV. Capacitance compensation and P/-8 leak subtraction were applied prior to recording ionic currents. To obtain the voltage-dependence of steady-state inactivation (SSI) and the corresponding VS movement (SSI F-V) curves cells were held at the conditioning potential for 200 ms and the available channel fraction was assessed by a depolarizing pulse to -20 mV. For gating currents P/4 subtraction was used with an interpulse holding potential of +40 mV.

VCF measurements

Oocytes were labeled with 10 μM methanethiosulfonate-carboxytetramethylrhodamine (MTS-TAMRA; Santa Cruz Biotechnology) in a depolarizing solution (mM: 110 KCl, 1.5 $MgCl_2$, 0.8 $CaCl_2$, 0.2 EDTA and 10 HEPES, pH 7.1) on ice for 20 min. MTS-TAMRA stock solution was 10 mM in DMSO and stored at −20°C. Illumination was provided by a green, high-powered LED (Luminus, PT-121) controlled through a driver

(Lumina Power, LDPC-30-6-24VDC) by the acquisition software to minimize photobleaching of the probe. The light was then focused into a liquid light guide with a 45°, 5mm compound parabolic concentrator (Edmund Optics) and the guide was coupled to the microscope via a collimating adapter (EXFO). A 40× water-immersion objective with a numerical aperture of 0.8 (CFI Plan Fluor, Nikon) was used. Light measurements were made with a photodiode (PIN-040A; United Detector Technology) mounted on an XY axis manipulator (Thorlabs Inc.) at the microscope epifluorescence port. The photodiode was attached to the integrating headstage of a patch-clamp amplifier (Axopatch-200A; Molecular Devices) for low noise amplification of the photocurrent. The fluorescence emission was focused onto the photodiode active area using an achromatic doublet (Thorlabs Inc.) with a focal distance of 25 mm.

Data analysis

For the analysis of fluorescence data, baseline fluorescence traces were recorded with no change of voltage during the illumination period. To correct for photobleaching, this baseline trace was filtered and subtracted from the fluorescence traces recorded during the application of the voltage protocol. The magnitude of fluorescence signals is expressed as $\Delta F / F_0$, where ΔF is the change in the signal amplitude in response to the voltage change and F_0 is the baseline fluorescence.

Steady-state G-V, SSI, F-V and SSI F-V curves were obtained by fitting the data points with a Boltzmann-function: $y = 1 / (1+ \exp[-(V-V_{1/2})/k)]$, where $V_{1/2}$ is the half-activation voltage and k is the slope factor. For direct comparison of current and VSD kinetics we used $t_{10\text{-}90\%}$ due to the different functions they follow. $t_{10\text{-}90\%}$ for current activation kinetics was determined by the time duration between the time points when the current reached 10 and 90 % of the peak value. For fluorescence signals with low signal to noise ratio $t_{10\text{-}90\%}$ determination was inaccurate, therefore for all fluorescence signals we calculated $t_{10\text{-}90\%C}$ from the time constants of single exponential fits (τ) to the signal by $t_{10\text{-}90\%C} = 2.197\tau$.

Valence-weighted F-V curves were calculated as $F(V)_w = (F(V)_1 \times z1 + F(V)_2 \times z2 + F(V)_3 \times z3 + F(V)_4 \times z4) / (z1 + z2 + z3 + z4)$, where $F(V)_I$ represents the F(V) function of the *i*th domain and z_i the valence of $F(V)_I$ determined from the Boltzmann-fit $y = 1 / (1+ \exp[-z\times(V-V_{1/2})/kT)$, where $V_{1/2}$ is the half-activation voltage and k is the Boltzmann-constant and T is temperature[3].

Statistical significance was attributed to $p<.05$ as determined by a two-tailed Student's t-test. For the comparison of multiple groups one-way ANOVA was applied and in the case of a significant difference it was followed by post-hoc Holm-Sidak pairwise comparisons among all groups or versus control. Errors in text and error bars in figures represent 95% confidence interval with number of trials (n) in parentheses.

References

1. Rudokas MW, Varga Z, Schubert AR, Asaro AB, Silva JR. The xenopus oocyte cut-open vaseline gap voltage-clamp technique with fluorometry. *J Vis Exp*. 2014
2. Stefani E, Bezanilla F. Cut-open oocyte voltage-clamp technique. *Methods Enzymol*. 1998;293:300-318.
3. Pantazis A, Savalli N, Sigg D, Neely A, Olcese R. Functional heterogeneity of the four voltage sensors of a human l-type calcium channel. *Proc Natl Acad Sci U S A*. 2014;111:18381-18386.

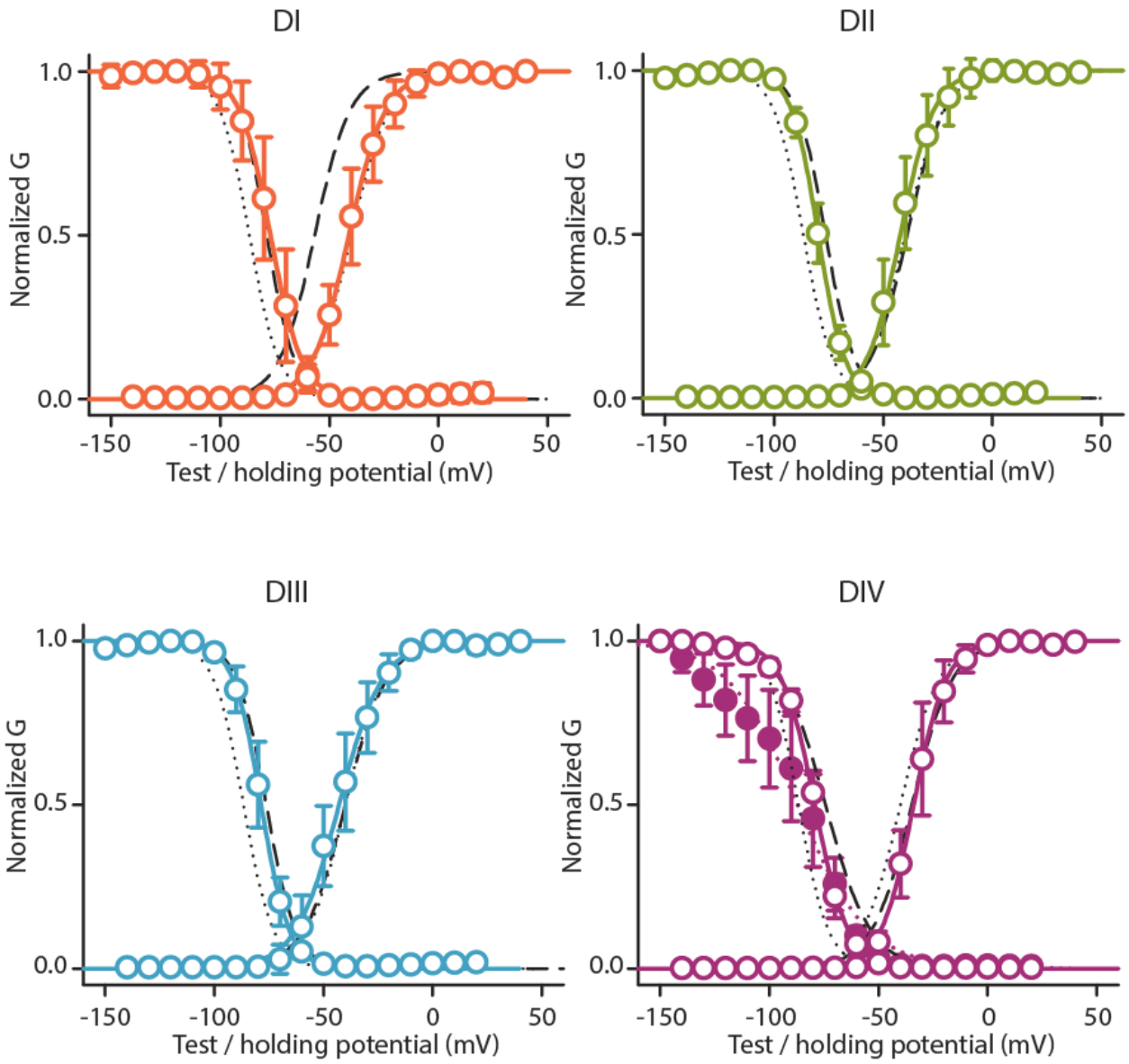

Figure S1. G-V and SSI functions of the unlabeled fluorescence constructs

G-V and SSI functions were obtained using the protocols described in the text from unlabeled LFS constructs (circles). Points represent mean ± 95CI from groups of 3 to 6 cells. The dotted line shows the WT-LFS data, while the dashed lines are curves from TAMRA-MTS labeled constructs. For DIV-LFS the SSI curve did not saturate at negative potentials (filled circles), but after DTT treatment (empty circles) approached the labeled channel.

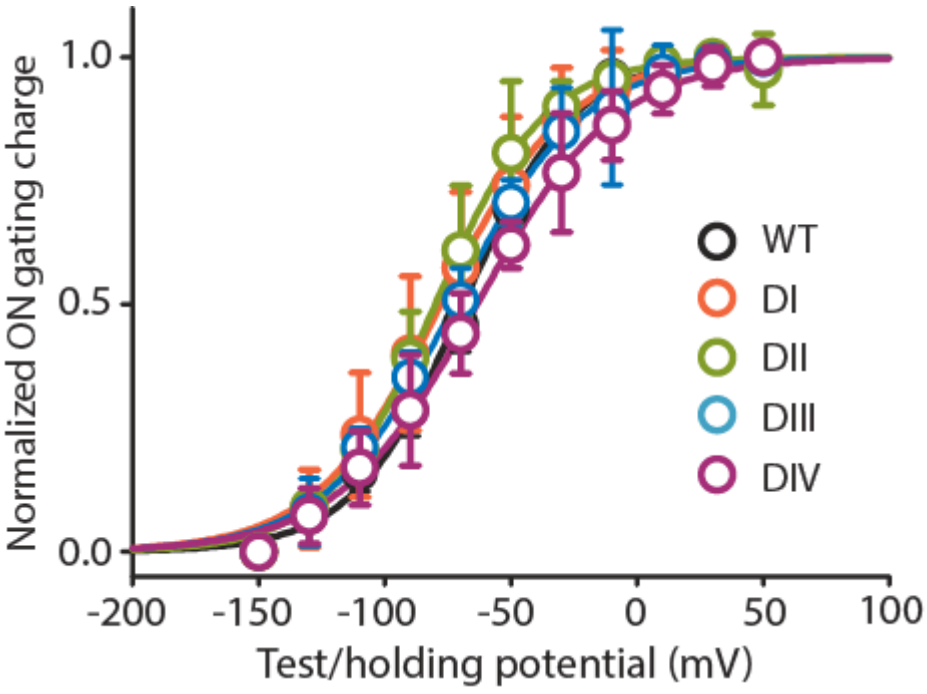

Figure S2. Comparison of integrated gating charge movement for WT-LFS and fluorescence constructs.

Voltage-dependence of integrated gating charge movement for WT-LFS, DI-LFS, DII-LFS, DIII-LFS and DIV-LFS channels. Gating currents were recorded during 20-ms depolarizing steps ranging from -150 to +50 mV in 20-mV steps. Capacitance and leak were removed using P/4 leak subtraction with a sub-sweep holding level of +40 mV. Gating currents were integrated for 10 ms following the voltage change. See **Table 1** in manuscript for parameters. Each point represents the mean ± 95CI from 4 to 7 cells.

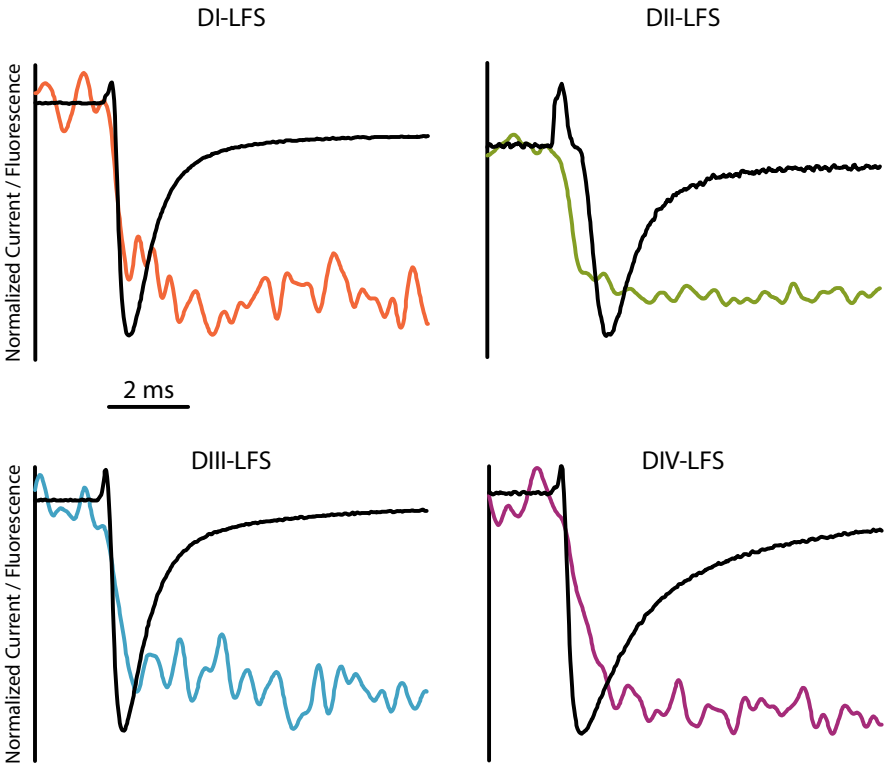

Figure S3. Comparison of ionic current and fluorescence kinetics in the four domains.

Na^+ currents and fluorescence signals were recorded from DI-LFS, DII-LFS, DIII-LFS and DIV-LFS channels to compare the kinetics of activation. Traces were recorded during a voltage step to +30 mV from -120 mV. The first 10 ms duration is shown.

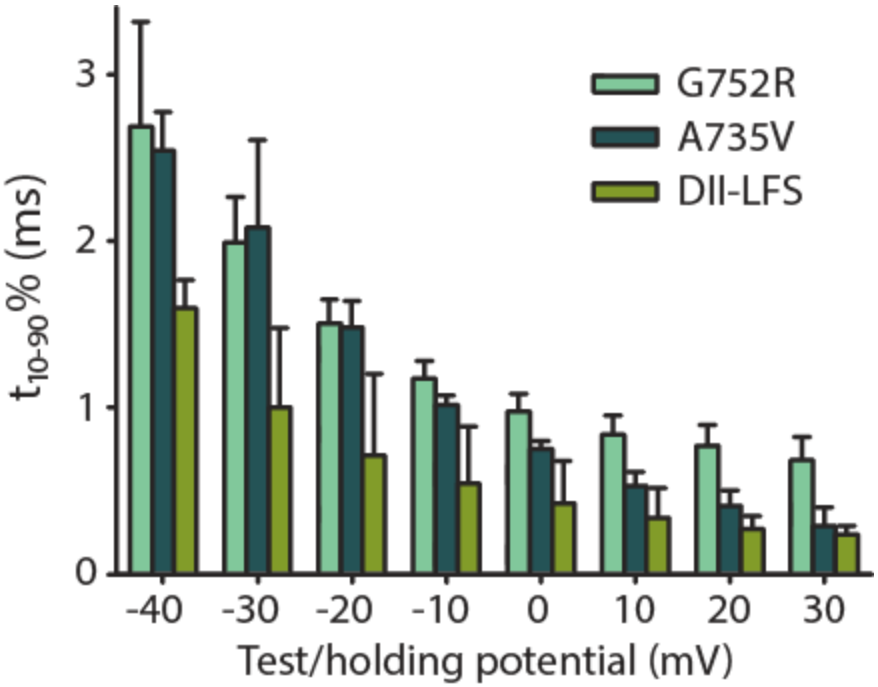

Figure S4. Comparison of ionic current activation kinetics of DII-LFS and the BrS mutants.

Activation kinetics were measured as $t_{10\text{-}90\%}$ rise time following a step to the indicated potentials from a prepulse of -120 mV for DII-LFS, DII-LFS-A735V and DII-LFS-G752R. Each point represents the mean ± 95CI from groups of 3 to 7 cells.

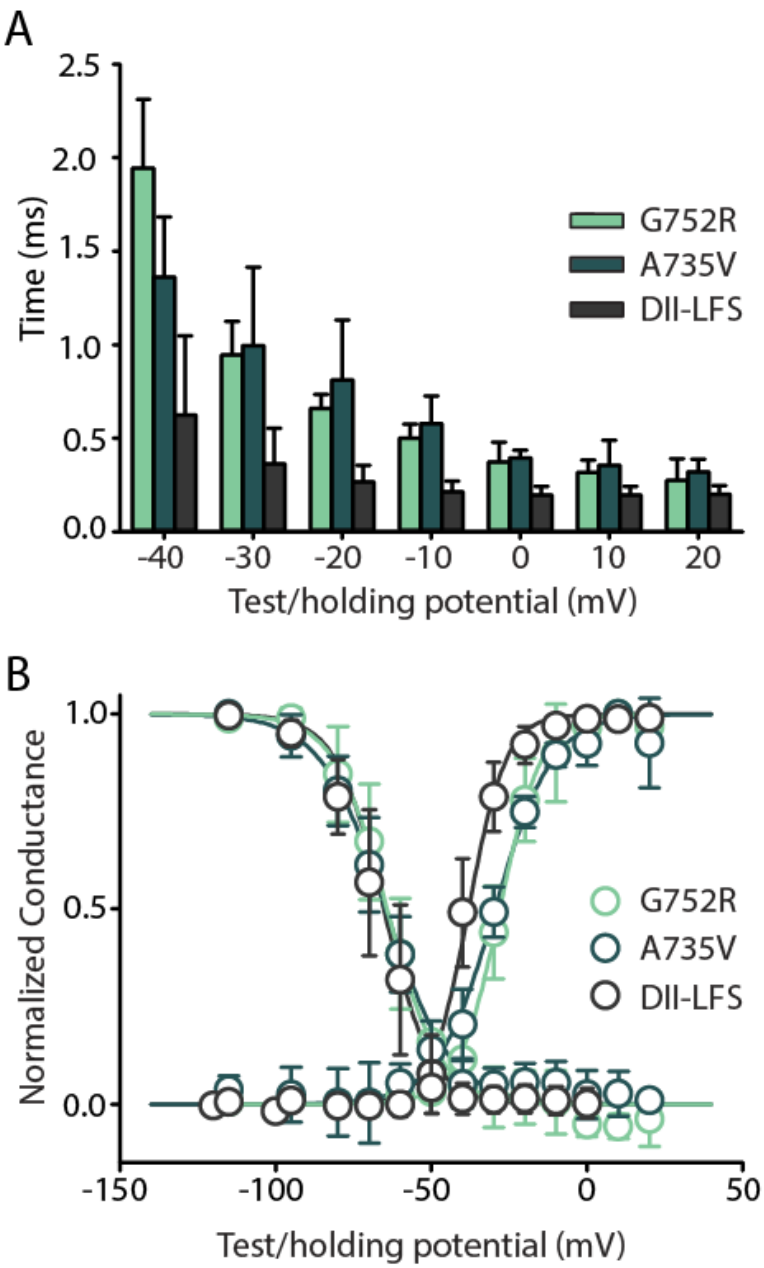

Figure S5: Steady-state inactivation, activation, and rise times for BrS mutants compared to wild-type expressed in HEK293T cells.

(A) Activation kinetics were measured as $t_{10\text{-}90\%}$ rise time following a step to the indicated potentials from a prepulse of -120 mV for WT (n=4), A735V (n=3), and G752R (n=4).

(B) Voltage-dependence of steady-state activation and steady-state inactivation curves for the WT, A735V, and G752R (purple, green, and red respectively). G-V curves were constructed from I-V relationships recorded from cells depolarized in 10 or 20 mV increments from a prepulse potential of -120 mV. Na^+ reversal potential was determined for each cell individually. For the SSI curves, cells were held at the conditioning potential ranging from -120 to +20 mV for 50 ms and the available channel fraction was assessed by a depolarizing pulse to -20 mV. Each point represents the mean ± 95CI from 4 to 11 cells.